



Solid–Liquid Phase Equilibrium: Alkane Systems for Low-Temperature Energy Storage

Maria C. M. Sequeira¹ · Bernardo A. Nogueira² · Fernando J. P. Caetano^{3,4} · Hermínio P. Diogo¹ · João M. N. A. Fareleira¹ · Rui Fausto^{2,5}

Received: 10 November 2023 / Accepted: 18 December 2023 / Published online: 1 February 2024
© The Author(s) 2024

Abstract

The thermal characterization of two binary systems of *n*-alkanes that can be used as Phase Change Materials (PCMs) for thermal energy storage at low temperatures is reported in this work. The construction of the solid–liquid binary phase diagrams was achieved using differential scanning calorimetry (DSC) and Raman spectroscopy. The *solidus* and *liquidus* equilibrium temperatures were determined using DSC for thirty-nine different samples, three for the pure *n*-alkanes and the remaining for binary mixtures at selected molar compositions and used to acquire the corresponding solid–liquid phase diagrams. The two binary systems of *n*-octane/*n*-decane (C_8/C_{10}) and *n*-decane/*n*-dodecane (C_{10}/C_{12}) are characterized by a eutectic behavior at low temperatures. The eutectic temperature for the system C_8/C_{10} was found at 211.95 K and the eutectic composition appeared at the molar fraction $x_{\text{octane}}=0.87$. For the system C_{10}/C_{12} , the eutectic temperature was found at 237.85 K, and the eutectic composition appeared for the molar fraction $x_{\text{decane}}=0.78$. This work aims to fulfill the lack of available data in the existing literature, considering the potential application of these systems for low-temperature thermal energy storage. Raman spectroscopy was used to complement the DSC data for the construction of the solid–liquid phase equilibrium diagrams, enabling the identification of the solid and liquid phases of the system. Additionally, the *liquidus* curve of the phase diagram was successfully described using a modified freezing point depression curve as fitting equation, the absolute root mean square deviation for the data correlation of the C_8/C_{10} and C_{10}/C_{12} systems being 2.56 K and 1.22 K, respectively. Ultimately, the fitting procedure also enabled a good prediction of the eutectic point for both studied systems.

Keywords Alkanes · Binary phase diagram · Energy storage · Eutectic · Phase change material (PCM)

The present article has been partially presented in the 22nd European Conference on Thermophysical Properties in Venice, Italy, 10th to 13th September 2023.

Extended author information available on the last page of the article

1 Introduction

The phase equilibrium studies for low-temperature energy storage applications in our group started with the work developed for the di-*n*-alkyl-adipates [1]. A new eutectic system was found and proved to be a good candidate as Phase Change Material (PCM) [1]. In this paper, two binary systems of *n*-alkanes are being presented also as eutectic systems suitable for cold thermal energy storage applications.

Energy storage has recently become an attractive technology due to the increasing use of renewable energies, many of which have an intermittent nature. Consequently, the continuous search for new materials that can be used for this purpose is crucial. Considering the different existing energy storage technologies, thermal energy storage has shown to be very promising since the world's primary energy generation is consumed or even wasted as heat [2–4]. For thermal energy storage, PCMs have been constantly proving to be one of the keys for large-scale applications of this technology [4–9].

PCMs can be categorized according to their chemical nature as inorganic, organic, and eutectics. Eutectics can then be classified as organic–organic, inorganic–inorganic, and inorganic–organic [10–12]. Organic PCMs have been widely used for thermal energy storage, in particular, *n*-alkanes, because of their singular phase transition performance, which relies on their high chemical stability, availability in a wide transition temperature range, low cost, long-term cyclic stability, and non-toxicity [6–8, 13, 14].

The use of PCMs involves several investigations, starting from the phase equilibrium studies, which are crucial to understand the thermal behavior of the materials, followed by the determination of thermophysical properties such as thermal conductivity, in order to understand if the materials conduct heat properly, and finally the evaluation of the performance of the materials to be used as PCMs [3, 5]. Several thermal performance studies have been carried out and reported in the literature focused on *n*-alkanes [3, 6–8, 15]. These studies provided evidence of the robustness of these type of compounds after submitted to several thermal stress cooling/heating cycles, reinforcing the choice for these materials in thermal energy storage applications.

Considering the final application of PCMs, another key aspect to consider when selecting the materials is the cost. For commercial applications, pure materials are usually more expensive when compared to blends, mainly industrial by-products [16]. The potential of industrial by-products is real, which is an important achievement to promote the circular economy and, when it is possible, the use of these products is indeed mandatory [16–18].

This work focuses on binary systems of *n*-alkanes that can be used for cold thermal energy storage applications. This is significantly important for the transportation of perishable consumables, mainly for medicines that need to be maintained at very low temperatures and are frequently temperature sensitive [11, 14]. In many instances, including this particular case, the PCM can be enclosed in a capsule in order to enable direct contact with the product to be cooled, avoiding eventual contaminations.

The binary systems studied in this work involve three *n*-alkanes, *n*-octane (*n*-C₈), *n*-decane (*n*-C₁₀), and *n*-dodecane (*n*-C₁₂). Studies of the two alkane systems included in this article, namely, the binary mixtures of C₈/C₁₀ and C₁₀/C₁₂, have previously been presented in the literature. The system C₈/C₁₀ was studied by Mondieig *et al.* [19] who have shown that for this system it is possible to identify a eutectic transformation, having also provided the corresponding temperatures of fusion for other compositions of the binary mixture. Furthermore, in that article [19], those authors published several other solid–liquid phase diagrams for alkane systems. However, the present system C₁₀/C₁₂ was not included. The latter system was previously studied by Espeau [20] and then by Ventolà *et al.* [21], but in those studies the temperatures and compositions do not seem to be clearly discernible. Regarding the enthalpy of fusion, no available data for these two systems, the knowledge of which is imperative for thermal energy storage applications could be found in the literature. Therefore, the present paper aims to complement the available data in the literature, reporting the temperature and enthalpy of fusion for several compositions of the two binary systems of *n*-alkanes under study, thus intending to be a significant contribution for the application of these materials to be phase change materials (PCM) for sub-zero energy storage applications.

2 Experimental

2.1 Materials

In this work, *n*-octane, *n*-decane, and *n*-dodecane were used as received. The water content of the materials used in this work was measured using a Karl-Fisher 831 KF Coulometer from Metrohm. Table 1 shows the characterization of the material samples used in this work.

Considering the high purity of the compounds as indicated on the analysis certificate provided by the supplier and on the analysis of water content levels determined just before the experimental measurements, the samples were used as received.

To achieve the highest accuracy in composition, the binary mixtures in this work were prepared gravimetrically using a Mettler Toledo MS205DU micro balance with a precision of ± 0.01 mg.

Table 1 Characterization of the liquids used in this work

Name	CAS number	Supplier	Lot Number	Water content (mg·kg ⁻¹)	Purity (mass fraction) (%)
<i>n</i> -octane	111-65-9	Thermo Scientific	10217841	25.6	99.3
<i>n</i> -decane	124-18-5	TCI Chemicals	OL5LO-XZ	19.8	100
<i>n</i> -dodecane	112-40-3	TCI Chemicals	F8JKF-TC	10.7	99.7

Purity as stated in the corresponding analysis certificate and water content measured in situ

2.2 Techniques

2.2.1 Differential Scanning Calorimetry (DSC)

The calorimetric measurements were performed with a 2920 MDSC system from TA Instruments Inc. The experimental procedure is described elsewhere [1]. Therefore, only a brief description is given here.

The sample masses of 3.0–10.0 mg were sealed in air inside aluminum pans and weighed with a precision of $\pm 0.1 \mu\text{g}$ by a Mettler UMT2 ultra-micro balance and analyzed by differential scanning calorimetry (DSC) at a scanning rate, $\beta = 5 \text{ }^\circ\text{C}\cdot\text{min}^{-1}$. Helium (Air Liquide N55) at a flow rate of $30 \text{ cm}^3\cdot\text{min}^{-1}$ was used as purging gas. The baseline was corrected by scanning along the temperature range of the experiments using an empty pan. The temperature and heat flow scales of the instrument were calibrated at different heating rates, based on the onsets of the fusion peaks of several standards. Details of the calibration procedure are described elsewhere [22].

2.2.2 Raman Spectroscopy

The present Raman spectra were acquired with a Horiba LabRam HR Evolution micro-Raman system using a solid-state laser ($\lambda = 532 \text{ nm}$, $\sim 50 \text{ mW}$) for excitation. The samples were probed with a $10\times$ objective, and the laser spot diameter on the sample was approximately $300 \mu\text{m}$. The system was calibrated using a Si crystal as reference (reference band at 520.5 cm^{-1}). The final spectra presented here represent the average of five spectra accumulations, with an acquisition time of 5 s and a resolution of 0.5 cm^{-1} . In the Raman experiments, the temperature-variation was carried out using a Linkam Scientific Instruments THMS 600 stage, which was controlled and measured by a T95-PE Linkpad controlling unit, the uncertainty in the temperature measurements being $< 0.01 \text{ }^\circ\text{C}$.

3 Results and Discussion

3.1 Binary System C_8/C_{10}

3.1.1 Differential Scanning Calorimetry (DSC)

DSC heating curves of the pure compounds, $n\text{-C}_8$ and $n\text{-C}_{10}$, and of some of the most significant binary mixtures are presented in Fig. 1. The relevant temperatures and enthalpies of fusion were obtained using the average values acquired from two consecutive cycles and are given in Table 2. The remaining DSC heating curves for all the other compositions, with the correspondent temperatures and enthalpies of fusion, are presented in the Supplementary Information (Fig. S1 and Table S1). The experimental *solidus* and *liquidus* temperature points were

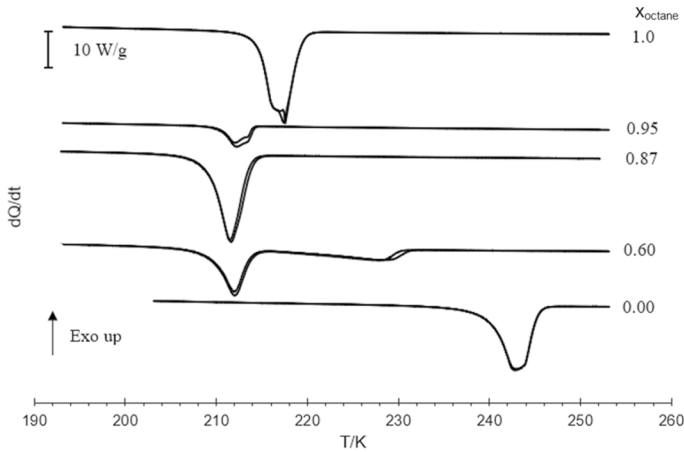


Fig. 1 DSC heating curves of $n\text{-C}_8$, $n\text{-C}_{10}$, and of selected binary mixtures, with selected octane molar fraction x_{octane} . The scanning rate was $\beta = 5 \text{ K}\cdot\text{min}^{-1}$

Table 2 DSC data of pure $n\text{-C}_8$, pure $n\text{-C}_{10}$, and three of their binary mixtures, including the onset temperatures, T_{onset} , maximum peak temperatures, T_{max} , and the corresponding enthalpies of fusion, at atmospheric pressure, 0.1 MPa

x_{octane}	DSC 1st peak			DSC 2nd peak		
	T_{onset} (K)	T_{max} (K)	$\Delta_{\text{fus}}H$ ($\text{J}\cdot\text{g}^{-1}$)	T_{onset} (K)	T_{max} (K)	$\Delta_{\text{fus}}H$ ($\text{J}\cdot\text{g}^{-1}$)
1	–	–	–	214.61	217.46	166.8
0.936	210.39	212.02	88.3*	–	214.91	–
0.874	–	–	–	210.21	211.94	138.7
0.598	209.48	211.98	79.9	218.74	228.39	40.3
0	–	–	–	240.19	242.93	169.4

Expanded uncertainties for a 95% confidence level ($k=2$): $U(x)=0.00008$; $U(T)=0.39 \text{ K}$; $U(\Delta_{\text{fus}}H)=4.7 \text{ J}\cdot\text{g}^{-1}$ (see Supplementary Information—S3)

*Overall enthalpy value for the two overlapped peaks

obtained from the maximum of the first and second endothermic peaks detected in the thermograms.

In Fig. 1, it is also possible to discern the different shape of the curves according to the molar composition of the binary mixture. In particular, the DSC curves of the binary mixtures show clear differences from the results for pure compounds and for the eutectic mixture. It is important to emphasize that the DSC curve for pure $n\text{-C}_8$ reveals a peak with a particular shape; notwithstanding, in the case of the eutectic mixture and pure $n\text{-C}_{10}$, only a single peak is identified to the fusion. On the contrary, for the mixture with molar fraction $x_{\text{octane}}=0.95$, an ill-defined peak is identified because of two overlapped peaks, and for the mixture $x_{\text{octane}}=0.60$, two distinct peaks are clearly visible.

Regarding the DSC thermograms, pure $n\text{-C}_8$ melts at $T_{fus}=217.46$ K with $\Delta_{fus}H=166.8$ J·g⁻¹ and $n\text{-C}_{10}$ melts at $T_{fus}=242.93$ K with $\Delta_{fus}H=169.4$ J·g⁻¹. The eutectic mixture corresponds to the molar composition $x_{octane}=0.87$ with $T_{fus}=212.53$ K and $\Delta_{fus}H=138.7$ J·g⁻¹.

For the construction of the binary solid–liquid phase diagram, these preliminary DSC results were confirmed using low-temperature Raman spectroscopy studies.

As mentioned before, Mondieig *et al.* [19] have previously published work on this binary system. In that important article, the reported melting temperatures of pure $n\text{-C}_8$ and $n\text{-C}_{10}$ were 216.6 K and 243.0 K, respectively. Thus, deviating by 0.86 K and -0.07 K, when compared to our experimental results for pure $n\text{-C}_8$ and $n\text{-C}_{10}$, respectively. We note that the deviation of the melting temperature of $n\text{-C}_{10}$ between the literature value and the present result is well within the estimated uncertainty of our data (see section S3 in the Supplementary information), as shown in Table 2. However, for $n\text{-C}_8$, the deviation slightly exceeds the uncertainty of our results. We did not find any indication of the uncertainty for the results of Mondieig *et al.* [19]. The differences for the temperatures of fusion can be justified by the thermal signature of this compound with a bimodal feature as discussed in Sections 3.2.1. and S4 in the Supplementary information for the studied n -alkanes.

3.1.2 Raman Spectroscopy

Raman spectra of pure $n\text{-C}_8$ and $n\text{-C}_{10}$ in both solid and liquid phases, of the binary mixture of the two alkanes having $x_{octane}=0.95$, and of the eutectic mixture for different temperatures are presented in Figs. 2, 3, 4, and 5, being the remaining Raman spectra shown in Figs. S3, S4, and S5 in the Supplementary Information.

The used Raman equipment allows to obtain images of the samples being investigated during the experiments, a feature that is particularly useful to additional monitoring of the system in real time and that allowed to corroborate visually the results obtained using DSC. These images are presented in Figs. 6 and 7 for the binary mixture with $x_{octane}=0.95$ and for the eutectic mixture, respectively; the surplus images

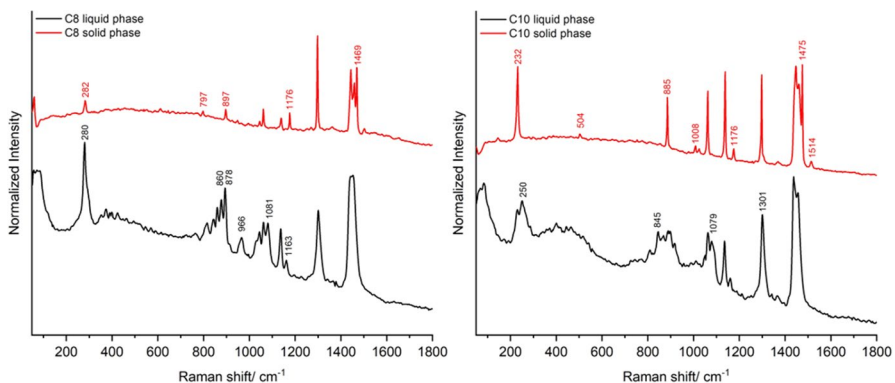


Fig. 2 Raman spectra of room-temperature liquid phase and cooled solid phase samples of pure $n\text{-C}_8$ and $n\text{-C}_{10}$, with marker bands in the 50–1800 cm⁻¹ range

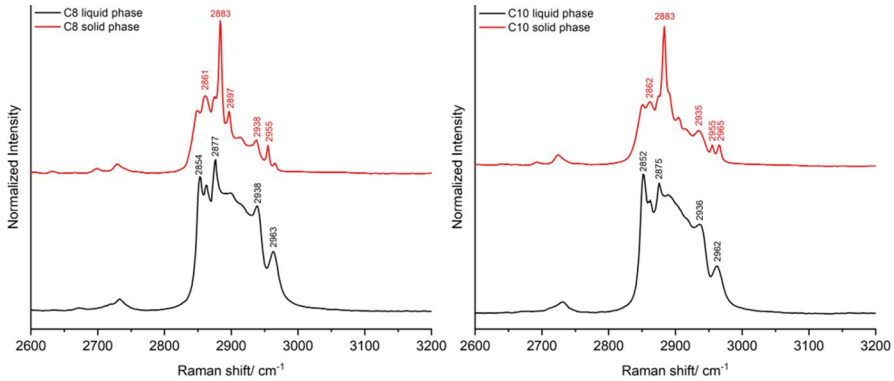


Fig. 3 Raman spectra of room-temperature liquid phase and cooled solid phase samples of pure n -C₈ and n -C₁₀, with marker bands in the 2600–3200 cm^{-1} range

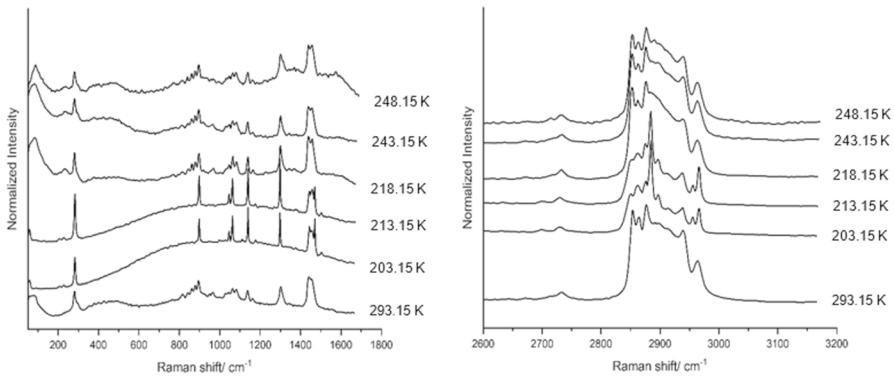


Fig. 4 Temperature-variation Raman spectra for the 95:5 C₈/C₁₀ binary mixture sample

for other mixtures are in the Supplementary Information in Figs. S10, S11, S12, and S13. The samples were cooled at $10 \text{ K}\cdot\text{min}^{-1}$ and heated at $5 \text{ K}\cdot\text{min}^{-1}$, which allows a direct comparison with the results obtained by DSC since the heating operating conditions were the same.

The results for pure n -C₈ and n -C₁₀ in solid and liquid states enable to identify the marker bands for each compound, making it possible to identify them in the prepared mixtures. It is therefore clear that the spectrum changes as a function of temperature and, for the eutectic mixture condition, a sharp peak typical of the melting point of a pure compound was observed, contrary to what was observed for other compositions, as $x_{\text{octane}}=0.95$, for example.

The identified characteristic bands for the pure compounds are the following: 280 cm^{-1} , 860 cm^{-1} , 878 cm^{-1} , 966 cm^{-1} , 1081 cm^{-1} , 1163 cm^{-1} , 2854 cm^{-1} , 2877 cm^{-1} , 2938 cm^{-1} , and 2963 cm^{-1} for the n -C₈ liquid phase; 282 cm^{-1} , 797 cm^{-1} , 897 cm^{-1} , 1176 cm^{-1} , 1469 cm^{-1} , 2861 cm^{-1} , 2883 cm^{-1} , 2897 cm^{-1} , 2938 cm^{-1} , and 2955 cm^{-1} for the n -C₈ solid phase; 250 cm^{-1} , 845 cm^{-1} , 1079 cm^{-1} , 1301

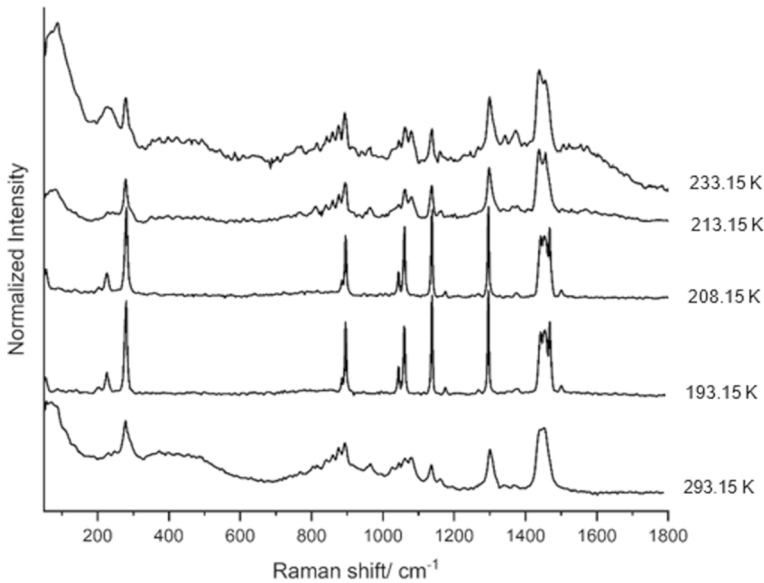


Fig. 5 Temperature-variation Raman spectra for the eutectic mixture of the C_8/C_{10} binary system

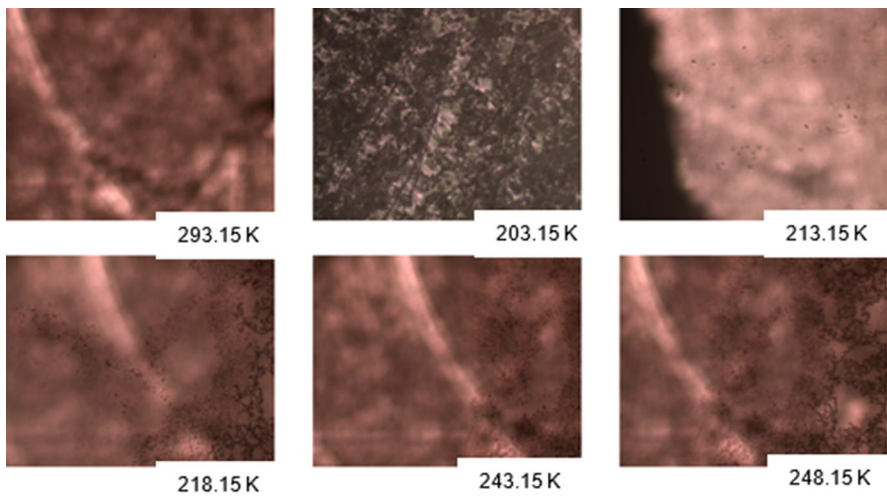


Fig. 6 95:5 C_8/C_{10} binary mixture photographs collected during the temperature-variation Raman spectroscopy experiment, with 10 \times magnification

cm^{-1} , 2852 cm^{-1} , 2875 cm^{-1} , 2936 cm^{-1} , and 2962 cm^{-1} for the $n\text{-}C_{10}$ liquid phase; and 232 cm^{-1} , 504 cm^{-1} , 885 cm^{-1} , 1008 cm^{-1} , 1176 cm^{-1} , 1475 cm^{-1} , 1541 cm^{-1} , 2862 cm^{-1} , 2883 cm^{-1} , 2935 cm^{-1} , 2955 cm^{-1} , and 2965 cm^{-1} for the $n\text{-}C_{10}$ solid phase.

The $x_{\text{octane}}=0.95$ binary system constituted by the two components in liquid phase was found to fully solidify at 203.15 K. At this temperature, the marker bands

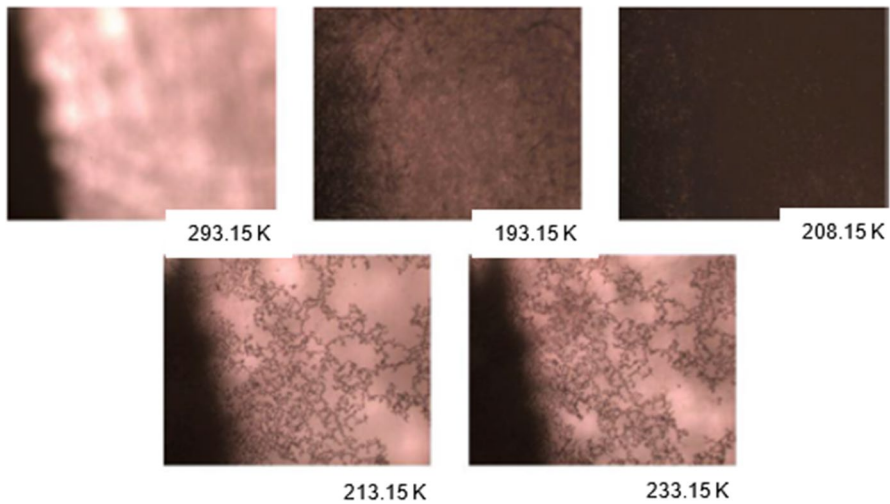


Fig. 7 Eutectic mixture of the binary system C_8/C_{10} photographs collected during the temperature-variation Raman spectroscopy experiment, with 10 \times magnification

of n - C_8 -solid phase at 282 cm^{-1} , 897 cm^{-1} , and 1470 cm^{-1} are observed in the Raman spectrum (Fig. 4), as well as the n - C_{10} -solid phase marker bands at 232 cm^{-1} and 885 cm^{-1} , confirming the n - C_8 -rich solid. At 213.15 K , some of the marker bands of n - C_8 -liquid phase, namely those at 878 cm^{-1} , 1081 cm^{-1} , and 1163 cm^{-1} start to be visible in the spectrum, indicating that n - C_8 -rich solid starts to melt at this temperature and the n - C_8 -rich liquid starts to be present in the mixture. The photographs collected during the experiment (Fig. 6) support the uncompleted melting of n - C_8 -rich solid at 213.15 K as detected in the DSC thermogram. Based on the Raman spectra, this phase transition appears to be completed at 218.15 K , where no more solid phase marker bands are visible.

The temperature-variation Raman experiment of the eutectic mixture shows that upon cooling, the sample was completely solidified at 193.15 K (n - C_8 -solid phase marker bands at 282 cm^{-1} , 897 cm^{-1} , and 1470 cm^{-1} , and n - C_{10} -solid phase marker bands at 232 cm^{-1} and 885 cm^{-1} can be identified in the spectrum), evidencing the n - C_8 -rich solid. At 208.15 K , the n - C_8 -liquid phase marker band at 1081 cm^{-1} starts to appear, being the phase transition of the binary mixture completed at 213.15 K , which is in accordance with the DSC results. The spectrum at 233.15 K shows the system in liquid phase.

3.2 Binary system C_{10}/C_{12}

3.2.1 Differential Scanning Calorimetry

DSC heating curves of the pure compounds, n - C_{10} and n - C_{12} , and of their most relevant binary mixtures are reported in Fig. 8. The corresponding temperatures and enthalpies of fusion, included in Table 3, were obtained from the average

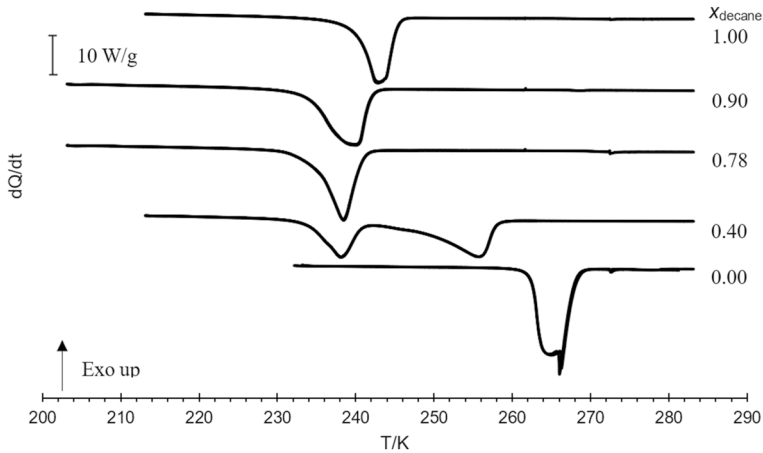


Fig. 8 DSC heating curves of n -C₁₀, n -C₁₂, and of different binary mixtures, with n -C₁₀ molar fraction x_{decane} , $\beta = 5 \text{ K} \cdot \text{min}^{-1}$

Table 3 DSC data for pure n -C₁₀, pure n -C₁₂, and their binary mixtures, including the onset temperatures, T_{onset} , maximum peak temperatures, T_{max} , and the corresponding enthalpies of fusion at atmospheric pressure, 0.1 MPa

x_{decane}	DSC 1st peak			DSC 2nd peak		
	T_{onset} (K)	T_{max} (K)	$\Delta_{\text{fus}}H$ (J·g ⁻¹)	T_{onset} (K)	T_{max} (K)	$\Delta_{\text{fus}}H$ (J·g ⁻¹)
1	—	—	—	240.19	242.93	169.4
0.900	233.88	237.60	—	—	240.06	143.0*
0.778	—	—	—	234.72	237.90	136.6
0.395	234.04	238.06	58.9	248.13	255.82	85.0
0	—	—	—	263.73	264.88	201.6

Expanded uncertainties for a 95% confidence level ($k=2$): $U(x)=0.00007$; $U(T)=0.39 \text{ K}$; $U(\Delta_{\text{fus}}H)=4.7 \text{ J} \cdot \text{g}^{-1}$ (see Supplementary Information—S3)

*Overall enthalpy value for the two overlapped peaks

values measured on two consecutive thermal cycles. The Supplementary information includes all the thermograms on heating and the corresponding temperatures and enthalpies of fusion (Fig. S2 and in Table S2, respectively). The experimental data for the melting temperature and enthalpy of pure n -C₁₀ were previously indicated, and for n -C₁₂, the T_{fus} is 264.88 K and $\Delta_{\text{fus}}H$ is 201.6 J·g⁻¹. The eutectic mixture corresponds to the molar proportion of $x_{\text{decane}}=0.78$ with $T_{\text{fus}}=237.90 \text{ K}$ and $\Delta_{\text{fus}}H=136.6 \text{ J} \cdot \text{g}^{-1}$.

As expected, the results shown in Fig. 8 allow to distinguish clear differences between the analyzed samples, both for pure compounds and for the binary mixtures, enabling to interpret these differences according to the molar composition of the binary mixtures. In the case of pure compounds, namely, n -C₁₀ and the eutectic mixture, only a single peak corresponding to the fusion is detected. In the case of n -C₁₂,

it is possible to identify a bimodal feature. This shape, observed for pure $n\text{-C}_{12}$ and previously for $n\text{-C}_8$ and $n\text{-C}_{10}$ (Section 3.1.1), is less well defined than those for the mixtures. In fact, for the heating ramp, the thermogram peaks for the pure components show unexpected double or noticeable asymmetric forms. A similar behavior has previously been observed by other authors, namely, Song *et al.* [23] for $n\text{-C}_{12}$. Those authors have developed an explanation essentially based on the shape/size of the crystals formed in the cool-down ramp [23]. Those effects would be hindered by the presence of a second component in the system. However, some polymorphism effects cannot be ruled out, although, resorting solely to the two techniques used in present work, it cannot be unambiguously confirmed. In addition, to the best of our knowledge, no reference in the specialized literature related to a polymorphic effect for the molecules under study was yet reported. Additionally, a supplementary study using DSC and different samples of pure $n\text{-C}_{12}$ to corroborate these results is presented in section S4 of the Supplementary Information. The observed behavior for those pure compounds indicates to be a genuine thermal signature of the studied n -alkanes. For the binary mixtures with $x_{\text{decane}}=0.90$, a broad peak, probably caused by the overlapping of two peaks, is observed, while for the binary mixture with $x_{\text{decane}}=0.40$, two distinct peaks are observed. These DSC results were further complemented and confirmed using low-temperature Raman spectroscopy to obtain the solid–liquid binary phase diagram of the system.

As mentioned, this binary system was previously studied by Espeau in 1995 [20] and then by Ventolà *et al.* in 2002 [21]; however, in those studies, the temperatures and compositions do not seem to be rigorously depicted. In this way, it is only possible to discern the general features of the *solidus* and *liquidus* lines, identify the eutectic behavior for this binary system, and recognize the similarity between the reported temperatures and compositions with our experimental results, including for the eutectic point.

3.2.2 Raman Spectroscopy

Raman spectra of pure $n\text{-C}_{12}$ in both solid and liquid phases, of the binary mixture having $x_{\text{decane}}=0.90$, and of the eutectic mixture for different temperatures are presented in Figs. 9, 10, and 11, respectively, being the remaining Raman spectra obtained for this binary system displayed in Figs. S7, S8, and S9 in the Supplementary Information. Additionally, the optical images of the sample collected during the Raman experiments are presented in Figs. 12 and 13, for the binary mixture with $x_{\text{decane}}=0.90$ and for the eutectic mixture, respectively; the surplus images for other mixtures are provided in the Supplementary Information (Figs. S14, S15, and S16). The same cooling and heating rates were applied as previously indicated for the $\text{C}_8\text{--C}_{10}$ binary system.

The results for pure $n\text{-C}_{12}$ in solid and liquid state enable to identify the marker bands for this compound, and together with the results previously presented for $n\text{-C}_{10}$ allow analyzing the data for the binary mixtures and distinguishing the different phases present in the mixture. Comparing the eutectic mixture with the system with overall composition $x_{\text{decane}}=0.90$, for example, it is possible to depict a different development of the spectra with the temperature, as was expected.

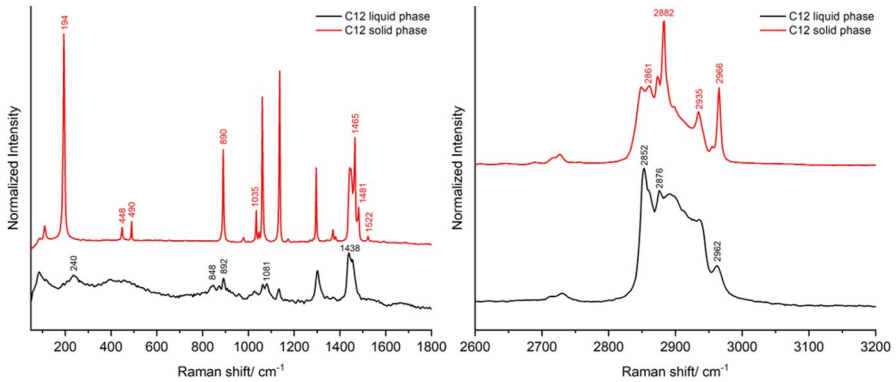


Fig. 9 Raman spectra of room-temperature liquid phase and cooled solid phase samples of pure n -C₁₂, with marker bands in the 50–1800 and in the 2600–3200 cm^{-1} ranges

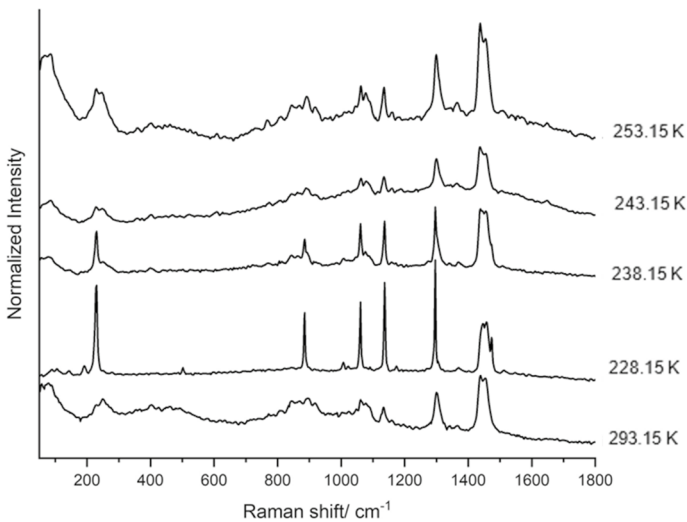


Fig. 10 Temperature-variation Raman spectra of the 90:10 C₁₀/C₁₂ binary mixture

The C₁₀/C₁₂ binary system with the ratio 90:10, starting with both components in the liquid phase, was observed to fully solidify at approximately 228.15 K. At this temperature, the liquid phase marker bands of the two components are no longer observed and the marker bands of the solid phases of n -C₁₀ (e.g., 232 cm^{-1} , 885 cm^{-1} , and 1475 cm^{-1}) and n -C₁₂ (e.g., 194 cm^{-1}) are clearly present in the spectrum. At 238.15 K, the intensity of the n -C₁₀ solid phase marker bands start to decrease, while the 250 cm^{-1} and 1079 cm^{-1} n -C₁₀ liquid phase marker bands arise, indicating the partial melting of this component. At 243.15 K, the n -C₁₀ is present almost only in its liquid phase, the marker bands for the solid phase being almost imperceptible, while both n -C₁₂ solid (e.g., 194 cm^{-1} and 1481 cm^{-1}) and liquid phase (e.g., 892

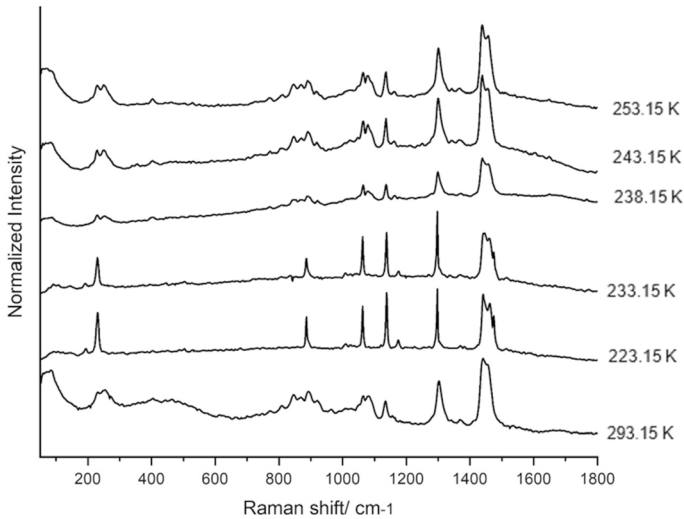


Fig. 11 Temperature-variation Raman spectra of the eutectic mixture of the C_{10}/C_{12} binary system

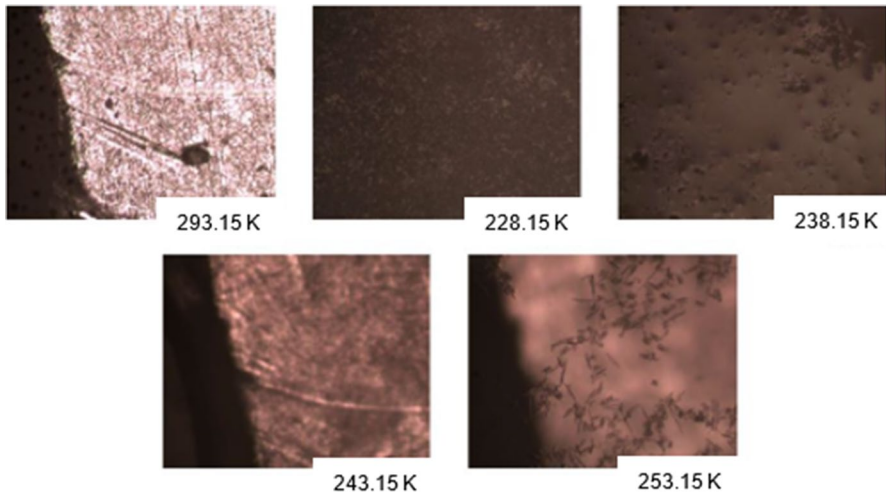


Fig. 12 90:10 C_{10}/C_{12} binary system photographs collected during the temperature-variation Raman spectroscopy experiment, with 10 \times magnification

cm^{-1}) marker bands are still observable in the spectrum. At 253.15 K, the binary mixture is completely melted.

The eutectic mixture crystallized completely at 223.15 K. The spectrum collected at this temperature presents the n - C_{10} solid phase marker bands (e.g., 232 cm^{-1} , 885 cm^{-1} , and 1475 cm^{-1}), as well as the n - C_{12} solid-state marker bands (e.g., 194 cm^{-1}). At 233.15 K, the melting of n - C_{10} is noticeable by the decreasing in the intensity of its solid-state Raman bands. At 238.15 K, those bands are no longer

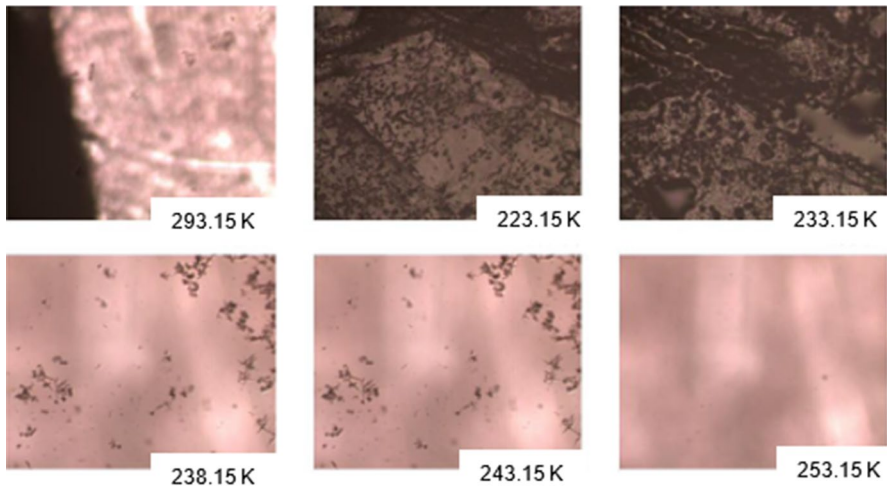


Fig. 13 Eutectic mixture of the binary system C_{10}/C_{12} photographs collected during the temperature-variation Raman spectroscopy experiment, with 10 \times magnification

observed, and are almost completely replaced by the Raman bands of the corresponding liquid phase (e.g., 250 cm^{-1}). The remaining solid phase melts between 243.15 K and 253.15 K, since at 243.15 K the solid-state marker band for $n\text{-}C_{12}$ 194 cm^{-1} is still identified in the spectrum (very low intensity) and, finally at 253.15 K, the solid phase marker bands for both compounds are no longer observed.

3.3 Solid–Liquid Binary Phase Diagrams

The DSC results for the maximum peak temperatures, T_{max} , were used to construct the binary solid–liquid phase diagrams for the systems C_8/C_{10} and C_{10}/C_{12} as shown in Figs. 14 and 15, respectively. The shape of the DSC curves does not allow to extract the T_{onset} values with confidence, as indicated in Tables S1 and S2. Therefore, T_{max} values were selected for the construction of the solid–liquid phase diagram. The DSC results used for the construction of those phase diagrams were complemented with low-temperature Raman spectroscopy data.

The solid–liquid binary phase diagram for the C_8/C_{10} system shown in Fig. 14 was obtained using the experimental results for nineteen different DSC experimental data points for the mixtures and other two for the pure components. It reveals a partially isomorphous eutectic system with a sharp melting point and two different biphasic zones where solid and liquid coexist: one liquid solution in equilibrium with different solid phases, having different compositions determined by the global composition of the system. Our results generally agree with those published by Mondieig *et al.* [19], where it is possible to observe a similar behavior of the *solidus* and *liquidus* lines. In addition, both the eutectic composition and the eutectic temperature obtained in the present work are commensurate with the results published by those authors.

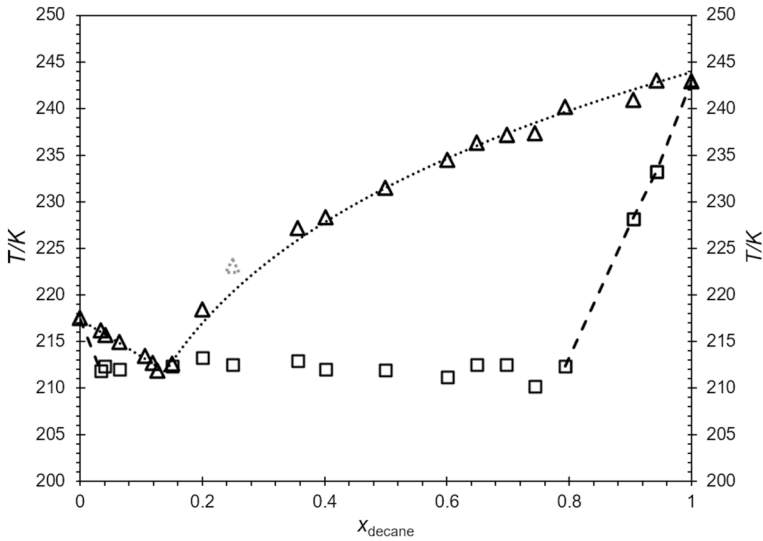


Fig. 14 Binary solid–liquid phase diagram of $n\text{-C}_8$ and $n\text{-C}_{10}$; \cdots fitted liquidus line, Δ experimental *liquidus* data points, \square experimental *solidus* data points; the gray dotted triangle ($x_{\text{decane}} \cong 0.25$) was not used the *liquidus* line fitting

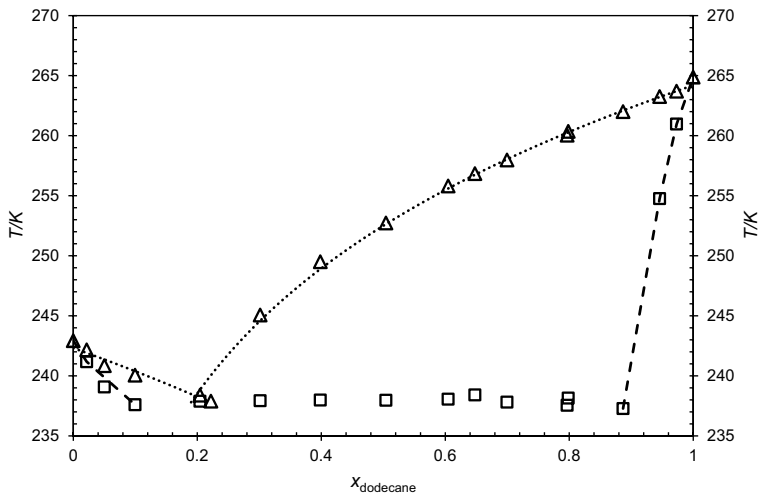


Fig. 15 Binary solid–liquid phase diagram of $n\text{-C}_{10}$ and $n\text{-C}_{12}$; \cdots fitted liquidus line, Δ experimental *liquidus* data points, \square experimental *solidus* data points temperature

The solid–liquid binary phase diagram presented in Fig. 15 for $\text{C}_{10}/\text{C}_{12}$ system was obtained using the experimental results for seventeen different molar fractions of the binary mixture and other two for the pure components, eighteen experimental points in total, revealing also a partially isomorphous eutectic behavior. The original

solid–liquid binary phase diagram for this system published by Espeau [20] in 1995 and then analyzed by Ventolà [21] again in 2002 is comparable with our experimental results. The coordinates for the eutectic point, that can be barely discerned in the graphic results of those authors, are commensurate with those of the present work, as well as the experimental temperatures and compositions, showing a similar behavior of the *liquidus* and *solidus* lines.

As previously described [1], it is possible to fit the *liquidus* curve of the solid–liquid binary phase diagrams using Eq. 1.

$$\ln\left(\frac{1}{x}\right) = a + b \cdot \frac{1}{T} \quad (1)$$

Equation 1 is a modification of the equation for the freezing point depression as described by Denbigh [24],

$$\ln\left(\frac{1}{x}\right) = \frac{L_{Mi}}{R} \left(\frac{1}{T} - \frac{1}{T_{Mi}} \right) \quad (2)$$

which is obtained assuming that an ideal liquid solution is in equilibrium with its pure solid solvent, with a temperature of fusion, T_{Mi} . Additionally, that equation assumes that the enthalpy of fusion of the pure solvent L_{Mi} does not depend on the composition of the mixture and that the specific heat capacity of the solid and the liquid solution is equal.

By comparing Eqs. 1 and 2, it is easy to obtain the following relations for the fitting coefficients a and b :

$$a = -\frac{L_{Mi}}{R} \cdot \frac{1}{T_{Mi}} \quad (3)$$

$$b = \frac{L_{Mi}}{R} \quad (4)$$

These relations would be correct if the conditions for Eq. 1 were valid. In our previous work on a system of di- n -alkyl adipates [1], Eq. 1 was successfully used as fitting equation to the experimental data to define the *liquidus* lines. An equivalent procedure has been used in the present work to define the *liquidus* lines for the solid–liquid phase diagrams for the systems C_8/C_{10} and C_{10}/C_{12} , which have been obtained by fitting Eq. 1 to the experimental data obtained by differential scanning calorimetry, with small deviations. These diagrams are shown in Figs. 14 and 15, for C_8/C_{10} and C_{10}/C_{12} , respectively. The coordinates of the eutectic point obtained by making use of the Eq. 1, as applied to both sides of the binary solid–liquid phase diagrams, are also in good agreement with the present experimental results.

However, it is to be noticed that the freezing point depression Eq. 2 [24] assumes that the solid in equilibrium with the liquid solution is one of the pure compounds present in the corresponding binary liquid solution. It is therefore expectable that such an equation may be adequate to describe the *liquidus* lines of a completely non-isomorphic eutectic system. However, as it can be observed

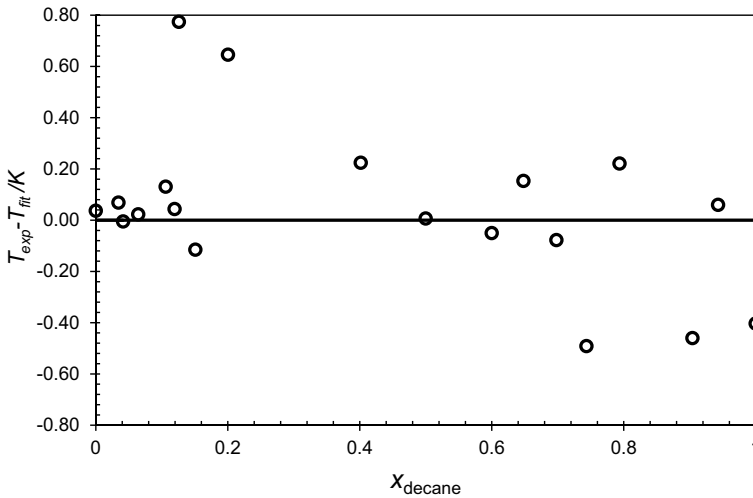


Fig. 16 Deviations of the experimental data obtained by thermal analysis, from the correlation fitting Eq. 1 for the *liquidus* line of the system C_8/C_{10} , as a function of n - C_{10} molar fraction

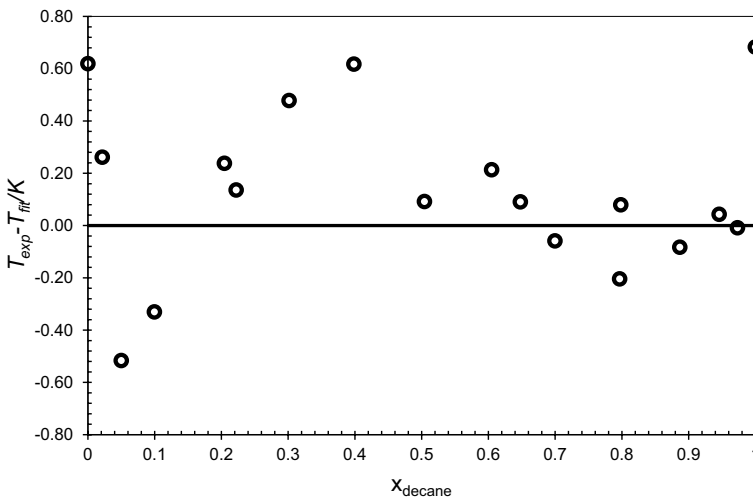


Fig. 17 Deviations of the experimental data obtained by thermal analysis, from the correlation fitting Eq. 1 for the *liquidus* line of the system C_{10}/C_{12} , as a function of n - C_{12} molar fraction

in Figs. 14 and 15, that will not be the case for the systems studied in the present work, which show partially isomorphic eutectic diagrams. This is evidenced by comparing those phase diagrams of the present work with that published in our previous paper for a eutectic system composed of two di- n -alkyl adipates. Therefore, the eventual benefits of using Eq. 1 as an empirical fitting equation to

describe the experimental data obtained for the *liquidus* lines of the *n*-alkane systems studied in the present work need to be further assessed.

In Figs. 16 and 17, it is possible to depict the deviations of the differential scanning calorimetry experimental data from the correlation equation used applying the parameters in Tables 4 and 5. The maximum absolute temperature deviation of all data is smaller than ± 0.80 K for both binary systems.

The statistical parameter, *rmsd*, used to describe the quality of the fitting of the binary solid–liquid phase diagrams in this work is defined in the Supplementary Information by Eq. S2.

From the values of the fitted parameters *a* and *b*, it is possible to estimate the average values for the melting enthalpy and the melting temperature of the mixtures, L_{Mi} and T_{Mi} , as previously shown [1]. In Tables 6 and 7, the values of L_{Mi} and T_{Mi} obtained by this fit are compared to the experimental values of $\Delta_{fus}H$ and T_{fus} for pure *n*-C₈, *n*-C₁₀, and *n*-C₁₂.

Furthermore, the eutectic composition and temperature were calculated using the same procedure described elsewhere [1]. For the first studied binary system, C₈/C₁₀, the fitted eutectic composition, x_{octane} , is 0.86 and the eutectic temperature is $T_{fus} = 211.76$ K, which corresponds to an absolute deviation of -0.18 K compared

Table 4 Fitted parameters *a* and *b* of Eq. 1, and the absolute root mean square deviation, *rmsd*, to the experimental *liquidus* data points using DSC, for the binary system C₈/C₁₀

Left side of the diagram			Right side of the diagram		
<i>a</i>	<i>b</i> (K)	<i>rmsd</i> (K)	<i>a</i>	<i>b</i> (K)	<i>rmsd</i> (K)
- 5.6696	1.2325×10^3	0.09	- 12.9655	3.1625×10^3	0.19

Table 5 Fitted parameters *a* and *b* of Eq. 1, and the absolute root mean square deviation, *rmsd*, to the experimental *liquidus* data points using DSC, for the binary system C₁₀/C₁₂

Left side of the diagram			Right side of the diagram		
<i>a</i>	<i>b</i> (K)	<i>rmsd</i> (K)	<i>a</i>	<i>b</i> (K)	<i>rmsd</i> (K)
- 13.1336	3.1824×10^3	0.25	- 14.9623	3.9530×10^3	0.14

Table 6 Comparison of the results obtained by fitting for L_{Mi} and T_{Mi} and the experimental results of $\Delta_{fus}H$ and T_{fus} , for pure *n*-C₈ and *n*-C₁₀, using the fitting parameters of Table 4

<i>n</i> -C ₈			<i>n</i> -C ₁₀		
L_{Mi} (J·g ⁻¹)	$\Delta_{fus}H$ (J·g ⁻¹)	Dev. (J·g ⁻¹)	L_{Mi} (J·g ⁻¹)	$\Delta_{fus}H$ (J·g ⁻¹)	Dev. (J·g ⁻¹)
89.7	166.8	77.1	184.8	169.4	- 15.4
<i>n</i> -C ₈			<i>n</i> -C ₁₀		
T_{Mi} (K)	T_{fus} (K)	Dev. (K)	T_{Mi} (K)	T_{fus} (K)	Dev. (K)
217.38	217.46	0.08	243.91	242.93	- 0.98

Table 7 Comparison of the results obtained by fitting for L_{Mi} and T_{Mi} and the experimental results of $\Delta_{fus}H$ and T_{fus} , for pure $n\text{-C}_{10}$ and $n\text{-C}_{12}$, using the fitted parameters, a and b , in Table 5

$n\text{-C}_{10}$			$n\text{-C}_{12}$		
L_{Mi} ($\text{J}\cdot\text{g}^{-1}$)	$\Delta_{fus}H$ ($\text{J}\cdot\text{g}^{-1}$)	Dev. ($\text{J}\cdot\text{g}^{-1}$)	L_{Mi} ($\text{J}\cdot\text{g}^{-1}$)	$\Delta_{fus}H$ ($\text{J}\cdot\text{g}^{-1}$)	Dev. ($\text{J}\cdot\text{g}^{-1}$)
186.0	169.4	- 16.6	193.0	201.6	8.6
$n\text{-C}_{10}$			$n\text{-C}_{12}$		
T_{Mi} (K)	T_{fus} (K)	Dev. (K)	T_{Mi} (K)	T_{fus} (K)	Dev. (K)
242.31	242.93	0.62	264.20	264.88	0.68

to the experimental result. Also, for the second binary system, $\text{C}_{10}/\text{C}_{12}$, the fitted eutectic composition, x_{decane} , is 0.80 and the eutectic temperature is $T_{fus} = 238.29$ K, which corresponds to an absolute deviation of 0.39 K compared to the experimental result. The absolute root mean square deviation, $rmsd$, of the experimental data points to the fitting equation for the *liquidus* line was determined as 0.13 K, for the system C_8/C_{10} , and as 0.08 K, for the system $\text{C}_{10}/\text{C}_{12}$. Therefore, the uncertainty is well within a 0.95 confidence level. Consequently, all the preceding comparisons give an indication that the use of Eq. 1 as fitting equation for the *liquidus* lines of both n -alkane systems was clearly successful.

4 Conclusions

Paraffin-based compounds have proven to be good candidates to be PCMs for thermal energy storage applications mainly because of their availability, reutilization, and relatively low cost. However, those applications have not been focused on low-temperature energy storage, and, therefore, the present work is a contribution to mitigate the fundamental research gap observed in cold-energy storage PCM systems.

In this work, two binary systems of n -alkanes, in particular, C_8/C_{10} and $\text{C}_{10}/\text{C}_{12}$, were characterized aiming their proposal to be used for low-temperature energy storage applications. Previous studies on these two systems were carried out by Espeau [20], Ventolà *et al.* [21], and Mondieig *et al.* [19], although with no relevant information provided for the applications concerning this paper. DSC measurements were carried out for thirty-seven different molar fractions of the binary mixtures and complemented with temperature-variation Raman spectroscopy studies allowing to obtain the complete solid–liquid phase diagrams for the two systems. The *liquidus* lines for both phase diagrams were correctly predicted using a fitting equation that has been previously applied [1] and has shown to be adequate to represent the present experimental data. The studied binary systems show a partially isomorphous eutectic behavior at low temperatures, the eutectic temperatures being found at 211.95 K for the C_8/C_{10} system and at 237.85 K for the $\text{C}_{10}/\text{C}_{12}$ system. For the C_8/C_{10} system, the eutectic composition has been found to be $x_{\text{octane}} = 0.87$ and the enthalpy of fusion was determined as $\Delta_{fus}H = 138.7\text{J}\cdot\text{g}^{-1}$. The $\text{C}_{10}/\text{C}_{12}$ system

presented a eutectic composition $x_{\text{decane}} = 0.78$ and the enthalpy of fusion was determined as $\Delta_{\text{fus}}H = 136.6 \text{ J}\cdot\text{g}^{-1}$.

Furthermore, the studied systems of *n*-alkanes gave important indications to possess good potential to be applied as PCM for thermal energy storage applications at low temperatures. In fact, these two systems can be used for different applications, according to their eutectic temperatures, nonetheless, with a reasonably high energy storage performance considering their latent heat of fusion, for such low temperatures.

As future work, the study of crucial thermophysical properties for practical applications in thermal energy storage as PCMs must be carried out for these two binary systems, particularly, their thermal conductivity.

Supplementary Information The online version contains supplementary material available at <https://doi.org/10.1007/s10765-023-03317-9>.

Acknowledgments This work was supported by Fundação para a Ciência e a Tecnologia (FCT), Portugal, Projects UIDB/00100/2020 (<https://doi.org/10.54499/UIDB/00100/2020>), UIDP/00100/2020 (<https://doi.org/10.54499/UIDP/00100/2020>), UIDB/00313/2020 (<https://doi.org/10.54499/UIDB/00313/2020>), UIDP/00313/2020 (<https://doi.org/10.54499/UIDP/00313/2020>) and IMS—LA/P/0056/2020/UIDB/00100/2020 (<https://doi.org/10.54499/LA/P/0056/2020>). M.C.M. Sequeira acknowledges the PhD grant funded by FCT ref. UI/BD/152239/2021.

Author Contributions MCMS participated in all the work, its execution and interpretation. BAN and RF participated in the Raman spectra and interpretation. HPD participated in the DSC and interpretation. FJPC, JMNAF and HPD participated in the organization of the experimental work and interpretation of the results. All authors participated in the writing of this paper.

Funding Open access funding provided by FCTIFCCN (b-on).

Data Availability Data will be made available on request.

Declarations

Competing interests The authors declare that they have no competing financial interest or personal relationships that could have appeared to influence the work reported in this paper.

Open Access This article is licensed under a Creative Commons Attribution 4.0 International License, which permits use, sharing, adaptation, distribution and reproduction in any medium or format, as long as you give appropriate credit to the original author(s) and the source, provide a link to the Creative Commons licence, and indicate if changes were made. The images or other third party material in this article are included in the article's Creative Commons licence, unless indicated otherwise in a credit line to the material. If material is not included in the article's Creative Commons licence and your intended use is not permitted by statutory regulation or exceeds the permitted use, you will need to obtain permission directly from the copyright holder. To view a copy of this licence, visit <http://creativecommons.org/licenses/by/4.0/>.

References

1. M.C.M. Sequeira, B.A. Nogueira, F.J.P. Caetano, H.P. Diogo, J.M.N.A. Fareleira, R. Fausto, Di-alkyl adipates as new phase change material for low. *Int. J. Thermophys.* **44**, 1–16 (2023). <https://doi.org/10.1007/s10765-023-03274-3>
2. A. Henry, R. Prasher, A. Majumdar, Five thermal energy grand challenges for decarbonization. *Nat. Energy* **5**, 635–637 (2020). <https://doi.org/10.1038/s41560-020-0675-9>

3. D. Lilley, A.K. Menon, S. Kaur, S. Lubner, R.S. Prasher, Phase change materials for thermal energy storage: a perspective on linking phonon physics to performance. *J. Appl. Phys.* **130**, 22 (2021). <https://doi.org/10.1063/5.0069342>
4. EASE, Thermal Energy Storage, Brussels (2023). <https://ease-storage.eu>
5. S.N. Gunasekara, S. Kumova, J.N.W. Chiu, V. Martin, Diagramme de phase expérimental du système dodécane–tridécano comme matériau à changement de phase pour des applications d'entreposage frigorifique. *Int. J. Refrig.* **82**, 130–140 (2017). <https://doi.org/10.1016/j.ijrefrig.2017.06.003>
6. H. Yan, H. Yang, J. Luo, N. Yin, Z. Tan, Q. Shi, Thermodynamic insights into n-alkanes phase change materials for thermal energy storage. *Chin. Chem. Lett.* **32**, 3825–3832 (2021). <https://doi.org/10.1016/j.ccl.2021.05.017>
7. S. Kahwaji, M.B. Johnson, A.C. Kheirabadi, D. Groulx, M.A. White, A comprehensive study of properties of paraffin phase change materials for solar thermal energy storage and thermal management applications. *Energy* **162**, 1169–1182 (2018). <https://doi.org/10.1016/j.energy.2018.08.068>
8. A. Anand, A. Shukla, A. Kumar, D. Buddhi, A. Sharma, Cycle test stability and corrosion evaluation of phase change materials used in thermal energy storage systems. *J. Energy Storage* **39**, 102664 (2021). <https://doi.org/10.1016/j.est.2021.102664>
9. D. Zhan, L. Zhao, Q. Yu, Y. Zhang, Y. Wang, G. Li, G. Lu, D. Zhan, M. Li, Phase change material for the cold storage of perishable products: from material preparation to material evaluation. *J. Mol. Liq.* **342**, 117455 (2021). <https://doi.org/10.1016/j.molliq.2021.117455>
10. C. Veerakumar, A. Sreekumar, Phase change material based cold thermal energy storage: materials, techniques and applications—a review. *Int. J. Refrig.* **67**, 271–289 (2016). <https://doi.org/10.1016/j.ijrefrig.2015.12.005>
11. Y. Lin, Y. Jia, G. Alva, G. Fang, Review on thermal conductivity enhancement, thermal properties and applications of phase change materials in thermal energy storage. *Renew. Sustain. Energy Rev.* **82**, 2730–2742 (2018). <https://doi.org/10.1016/j.rser.2017.10.002>
12. D. Zhou, C.Y. Zhao, Y. Tian, Review on thermal energy storage with phase change materials (PCMs) in building applications. *Appl. Energy* **92**, 593–605 (2012). <https://doi.org/10.1016/j.apenergy.2011.08.025>
13. S. Sarkar, S. Mestry, S.T. Mhaske, Developments in phase change material (PCM) doped energy efficient polyurethane (PU) foam for perishable food cold-storage applications: a review. *J. Energy Storage* **50**, 104620 (2022). <https://doi.org/10.1016/j.est.2022.104620>
14. G. Li, Q. Yu, Y. Liu, M. Li, Y. Zhang, Y. Wang, The efficient and developing phase transition freezing materials generated from amino acids. *J. Mol. Liq.* **382**, 121933 (2023). <https://doi.org/10.1016/j.molliq.2023.121933>
15. C. Alkan, A. Sari, A. Karaipekli, Preparation, thermal properties and thermal reliability of microencapsulated n-eicosane as novel phase change material for thermal energy storage. *Energy Convers. Manag.* **52**, 687–692 (2011). <https://doi.org/10.1016/j.enconman.2010.07.047>
16. S.N. Gunasekara, V. Martin, J.N. Chiu, Phase equilibrium in the design of phase change materials for thermal energy storage: state-of-the-art. *Renew. Sustain. Energy Rev.* **73**, 558–581 (2017). <https://doi.org/10.1016/j.rser.2017.01.108>
17. S. Khare, M. Dell'Amico, C. Knight, S. McGarry, Selection of materials for high temperature latent heat energy storage. *Sol. Energy Mater. Sol. Cells* **107**, 20–27 (2012). <https://doi.org/10.1016/j.solmat.2011.07.047>
18. J. Yagi, T. Akiyama, Storage of thermal energy for effective use of waste heat from industries. *J. Mater. Process. Technol.* **48**, 793–804 (1995). [https://doi.org/10.1016/0924-0136\(94\)01723-E](https://doi.org/10.1016/0924-0136(94)01723-E)
19. D. Mondieig, F. Rajabalee, V. Métivaud, H.A.J. Oonk, M.A. Cuevas-Diarte, n-Alkane binary molecular alloys. *Chem. Mater.* **16**, 786–798 (2004). <https://doi.org/10.1021/cm031169p>
20. P. Espeau, Synchronisation dans la famille des alcanes de C8H18 à C17H36 : conception, élaboration et caractérisation de nouveaux matériaux à changement de phase à base d'alliages moléculaires (MCPAM) : application à la protection thermique dans le domaine agro-a, Université Bordeaux I (1995)
21. L. Ventolà, T. Calvet, M.Á. Cuevas-Diarte, V. Métivaud, D. Mondieig, H. Oonk, From concept to application. A new phase change material for thermal protection at -11 °C. *Mater. Res. Innov.* **6**, 284–290 (2002). <https://doi.org/10.1007/s10019-002-0213-3>
22. J.J. Moura Ramos, R. Taveira-Marques, H.P. Diogo, Estimation of the fragility index of indomethacin by DSC using the heating and cooling rate dependency of the glass transition. *J. Pharm. Sci.* **93**, 1503–1507 (2004). <https://doi.org/10.1002/jps.20061>

23. Y. Song, N. Zhang, Y. Jing, X. Cao, Y. Yuan, F. Haghighat, Experimental and numerical investigation on dodecane/expanded graphite shape-stabilized phase change material for cold energy storage. *Energy* **189**, 116175 (2019). <https://doi.org/10.1016/j.energy.2019.116175>
24. K. Denbigh, *Principles of Chemical Equilibrium*, 2nd edn. (Cambridge University Press, London, 1966)

Publisher's Note Springer Nature remains neutral with regard to jurisdictional claims in published maps and institutional affiliations.

Authors and Affiliations

Maria C. M. Sequeira¹  · Bernardo A. Nogueira²  · Fernando J. P. Caetano^{3,4}  ·
Hermínio P. Diogo¹  · João M. N. A. Fareleira¹  · Rui Fausto^{2,5} 

✉ Fernando J. P. Caetano
fcaetano@uab.pt

- ¹ Centro de Química Estrutural, Institute of Molecular Sciences, Departamento de Engenharia Química, Instituto Superior Técnico, Universidade de Lisboa, Av. Rovisco Pais, 1049-001 Lisbon, Portugal
- ² Departamento de Química, CQC-IMS, Universidade de Coimbra, 3004-535 Coimbra, Portugal
- ³ Departamento de Ciências e Tecnologia, Universidade Aberta, 1269-001 Lisbon, Portugal
- ⁴ Centro de Química Estrutural, Institute of Molecular Sciences, Instituto Superior Técnico, Universidade de Lisboa, Av. Rovisco Pais, 1049-001 Lisbon, Portugal
- ⁵ Department of Physics, Faculty of Sciences and Letters, Istanbul Kultur Univ., Ataköy Campus, Bakirköy, 34156 Istanbul, Turkey